IOPscience iopscience.iop.org

Home Search Collections Journals About Contact us My IOPscience

Fast-atom diffraction at surfaces

This content has been downloaded from IOPscience. Please scroll down to see the full text.

2009 J. Phys.: Conf. Ser. 194 012057

(http://iopscience.iop.org/1742-6596/194/1/012057)

View the table of contents for this issue, or go to the journal homepage for more

Download details:

IP Address: 158.64.77.122
This content was downloaded on 11/10/2013 at 18:11

Please note that terms and conditions apply.

Journal of Physics: Conference Series **194** (2009) 012057 doi:10.1088/1742-6596/194/1/012057

Fast-Atom Diffraction at Surfaces

F Aigner[1], N Simonović[1,2], B Solleder[1], L Wirtz[3] and J Burgdörfer[1]

[1] Institute for Theoretical Physics, Vienna University of Technology, A-1040 Vienna, Austria, EU

[2] Institute of Physics, P.O. Box 57, 11001 Belgrade, Serbia

[3] IEMN, CNRS, Villeneuve d'Ascq, France, EU

E-mail: florian.aigner@tuwien.ac.at

Abstract. Fast helium atoms diffracted at alkali-halide surfaces under grazing angles of incidence exhibit intriguing diffraction patterns. The persistence of quantum coherence is remarkable, considering high surface temperatures and high (keV) kinetic energies of the incident atoms. Dissipative and decohering effects such as the momentum transfer between the incident helium atoms and the surface influence the diffraction patterns and control the width of the diffraction peaks, but they are weak enough to preserve the visibility of the diffration patterns. We perform an ab initio simulation of the quantum diffraction of fast helium beams at a LiF (100) surface in the ⟨110⟩ direction. Our results agree well with recent experimental diffraction data.

1. Introduction

Scattering of particles at surfaces can be used to illustrate the quantum wave nature. In their pioneering experiments, Estermann and Stern [1], observed interference patterns of slow ("thermal") helium atoms and H_2 molecules scattered off alkali halide surfaces. The de Broglie wavelength used in these experiments was still relatively large - typically in the order of the lattice constant of the target surface.

More recently, the wave nature of massive particles has been very impressively demonstrated in a variety of multi-path interference experiments. Using double slits or gratings, interference of remarkably massive objects like fullerenes been studied successfully [2, 3]. In matter-wave interferometry of large and complex biomolecules, de Broglie wavelengths as small as few picometers ($10^{-12}\,m$) have been reached [3]. Today, the same regime of very small de Broglie wavelengths $\lambda_{dB} \to 0$, can be approached not only by scattering heavy particles, but also by using lighter particles with a considerably higher kinetic energy. Sub-picometer wavelengths have been accessed by scattering studies of fast atoms with keV energies at surfaces [4, 5, 6] with λ_{dB} as small as ≈ 200 femtometers. In spite of the remarkably small wavelength, the diffraction patterns obtained by these experiments do not only show clear evidence of coherent wavepacket interference, but even provide detailed structural information about the surface. This is all the more remarkable, as thermal fluctuation amplitudes of the surface atoms are much larger than λ_{dB}. The width (and thus the visibility) of the peaks in the resulting diffraction patterns is directly connected to the coherence length of the incident particle. The number of unit cells coherently illuminated by the particle controls the shape of the diffaction peaks in much the same way as the number of slits of a grating illuminated in a multi-slit experiment. The coherence is limited as "which path" information is encoded in the wave function. Phonon

© 2009 IOP Publishing Ltd

wavepackets which are locally excited in the surface contain information on the localization of the interaction between incident atom and the surface. This has the same decohering effect as extracting information on the localization of a particle passing through a slit.

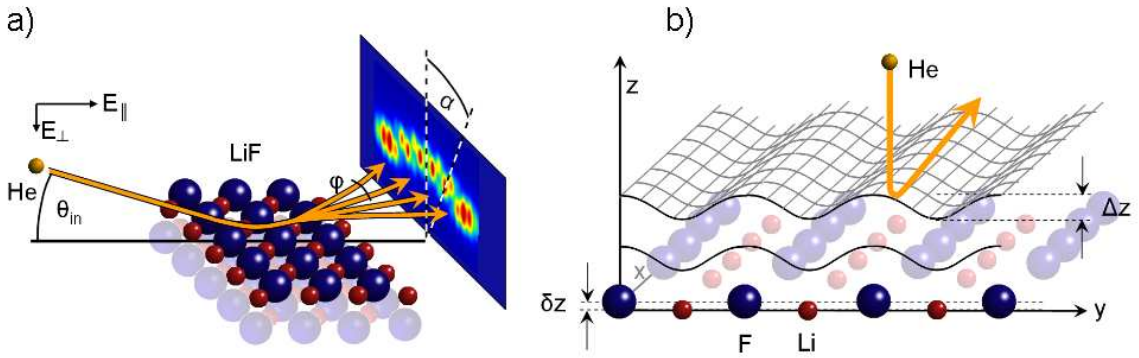

Figure 1. Helium atoms scattered at the LiF-surface at a grazing angle of incidence θ (a). In 100-direction, the He atoms interact with longitudinal chains of either Li or F atoms (b). Averaging the He-LiF potential along the longitudinal direction yields an effective two-dimensional potential.

In this communication we present examples of ab initio simulations of fast helium atom diffraction (^{4}He) at a LiF(100) surface. We analyze the suppression of decoherence in grazing-incidence scattering within an open quantum system (OQS) approach and quantitatively reconstruct experimental diffraction images [4, 5, 7].

2. Method

Fast atom scattering at surfaces under small grazing angles ($\theta_{in} \approx 1°$) is characterized by widely disparate kinetic energies parallel (Fig. 1a) ($E_\parallel = E_0 \cos^2\theta_{in} \approx E_0$) and normal ($E_\perp = E_0 \sin^2\theta_{in} \approx E_0\,\theta_{in}^2$) to the surface. This leads to vastly different projected de Broglie wavelengths

$$\lambda_{dB\,\perp,\parallel} = 2\pi/k_{\perp,\parallel} = 2\pi\hbar/\sqrt{2ME_{\perp,\parallel}}, \tag{1}$$

where $k_\parallel = k_x$ and $k_\perp = k_z$ are parallel and normal components of the wave vector of the incident beam, respectively. While $\lambda_{dB\perp}$ is comparable to the lattice spacing ($a = 2.01$Å for LiF) $\lambda_{dB\,\parallel}$ is orders of magnitude smaller. The fast motion along the surface leads to an approximate separability of the longitudinal and the transverse degrees of freedom and a weak coupling during the collision between them [8]. By averaging the atom-surface potential along the direction of the incident atom (x-direction), the scattered particle experiences an effective two-dimensional atomic string potential $V_{str}(y,z)$ (Fig. 1b).

Projecting the outgoing wave onto the plane transverse to the beam direction $|\langle k_y k_z|\Psi_{out}\rangle|^2$, two-dimensional diffraction patterns (see Fig. 1a) emerge. The remarkable persistence of quantum coherence in the presence of an energetic collision with keV energies and lattice vibrations at elevated temperatures in the experiment ($T \approx 620$ K [4, 6]) is the key to quantitatively analyzing diffraction patterns and extracting structural and dynamical information.

Starting point of the open quantum system approach (OQS) [2] is the reduction of the Liouville-von Neumann equation

$$i\frac{d\rho(t)}{dt} = [H, \rho(t)]\ , \tag{2}$$

for the density operator ρ of the entangled system of atomic wavepacket and surface to a Lindblad equation

$$\frac{d\sigma(t)}{dt} = -i\,[H_S, \sigma(t)] + \hat{R}\sigma(t)\,, \tag{3}$$

for the reduced density operator

$$\sigma(t) = Tr_R\,[\rho(t)] = \sum_i \{i|\rho(t)|i\}\ , \tag{4}$$

describing the translational motion of the atomic wavepacket where all "reservoir" degrees of freedom (R) representing the LiF surface have been traced out. The partial trace in Eq. (4) includes both the average over thermal excitation of the surface as well as collisional excitations of the surface by the interacting beam, which is the root cause for decoherence represented in Eq. (3) by the so-called relaxation operator $\hat{R}$.

Under surface channeling conditions, the longitudinal motion is to a good degree of approximation decoupled from other degrees of freedom (except for cases of resonant coherent excitations [15], i. e. frequency matching of the longitudinal corrugation with internal degrees of freedom of the projectile). We therefore separate the system Hamiltonian H_S in longitudinal and transverse parts

$$H_S = \frac{P_\perp^2}{2m} + V_{str}(y,z) + \frac{P_\parallel^2}{2m}, \tag{5}$$

where $P_\parallel$ is the momentum in the x-direction, the fast component of the particle motion, and $P_\perp$ is the momentum parallel to the detector plane (y,z).

The Hamiltonian contains the effective transverse interaction potential of atom with the LiF surface, $V_{str}(y,z)$. It is obtained by averaging the full potential $V_{surf}(\vec{r})$

$$V_{str}(y,z) = \frac{1}{d}\int_{x_0}^{x_0+d} dx\, V_{surf}(x,y,z)\,, \tag{6}$$

where d is the lattice space.

The initial density matrix of the atomic beam prior to entanglement with the solid,

$$\sigma(t=0) = \int d^3p_i\, |\Psi_{\vec{p_i}}\rangle\langle\Psi_{\vec{p_i}}| \tag{7}$$

corresponds to an integral over wavepackets representing the incoherent energy- and angular spread of the initial beam.

In the presence of an environment with a very large number of degrees of freedom, the quantum-to-classical crossover can be understood within the framework of decoherence theory [1, 9, 10]. We solve the Lindblad equation by a quantum trajectory Monte Carlo (QTMC) method [11] which is an extension of similar techniques in quantum optics [13]. In the present case of free-particle wavepackets, the QTMC reduces to an ensemble average over solutions of a stochastic linear Schrödinger equation. The evolution of the wavepacket is given by a sequence of collisions and propagation in the effective potential. Each stochastic realization of the wavepacket at the time $t = t_N$ is given by

$$|\Psi_i(t)\rangle = \prod_{j=1}^{N} U_{coll}\,(\vec{q}_j, t_j)\, U_{cont}\,(t_j, t_{j-1})\,|\Psi_i\rangle\,, \tag{8}$$

where $|\Psi_i\rangle$ is the initial wavepacket at $t_0 = 0$. The evolution operator for an impulsive stochastic collisional momentum exchange $\vec{q}_j$ with the surface is given by

$$U_{coll}\,(\vec{q}_j, t_j) = \exp\,(i\vec{q}_j\vec{r})\ , \tag{9}$$

while the continuous evolution in between two "kicks" during the interval $[t_j, t_{j-1}]$ is given by

$$U_{cont}\left(t_j, t_{j-1}\right) = \exp\left(-iH_S\left(t_j - t_{j-1}\right)\right) , \tag{10}$$

with the system Hamiltonian H_S.

Momentum transfers $\{\vec{q}_j\}$ as well as collision times $\{t_j\}$ are stochastic sequences determined by collisional interactions with the environment. The resulting diffraction pattern in the transverse plane results from an ensemble average over stochastic realizations.

The momentum transfer distribution functions in longitudinal (x-) direction and in the transverse (y, z-) directions entering Eq. 9 are obtained along sequences of binary collisions between helium and lithium and fluorine by averaging over the random displacement of the thermally excited lattice atoms.

Diffraction images can be reconstructed only when decay of coherence across the beam profile due to encoding of localization information ("which path" information) is accounted for. Neglecting first the initial beam divergence, we consider an incident Gaussian wavepacket (Fig. 3) of the form

$$\Psi_{in}(\vec{r}) = e^{ik_{\parallel}x}\,\Psi_{\perp}(y,z) \tag{11a}$$

with

$$\Psi_{\perp}(x,y) \propto e^{-ik_{\perp}z} e^{-y^2/2\sigma_y^2} e^{-(z-z_0)^2/2\sigma_z^2} . \tag{11b}$$

$\sigma_{y,z}$ are the transverse coherence length of the incident beam determined by the width of the zeroth-order diffraction peak ($\sigma_y^{in} = \sigma_x^{in} \approx 2L\frac{\lambda_{dB\parallel}}{D}$). The latter is controlled by the collimation slit of width D positioned at a distance L in front of the surface. The transverse coherence length is large compared to the lattice spacing. In fact, Eq. (11) is close to a delocalized plane wave. We expand the initial wavepacket in terms of a coherent superposition of narrow Gaussian wavepackets (Fig. 3a) each of which is propagated according to Eqs. (8 to 10). The random evolution phases acquired due to collisions occuring at different instances in time (i. e. different x coordinates along the string) causes a reduction of the transverse coherence length (Fig. 3b) along the surface normal, σ_z^{out}, of the projected wavepacket, monitored after its center reached distance from the surface $z = z_0$ again.

Two portions of the wave packet which are initially separated by the offset δz hit the surface at different positions on the longitudinal (x-) axis (see Fig. 2). If both trajectories suffer the same amount of momentum transfer δk during the impact on the surface, their phase difference after the impact is $\phi \approx \delta k \delta x$. Only if $\phi \ll 2\pi$, the two paths will interfere constructively. The coherence width of the wavepacket in z-direction (perpendicular to the surface) can therefore be roughly estimated as

$$\delta z = \delta x/\theta_{in} \approx \pi\theta_{in}/\delta k \tag{12}$$

With $\delta k \approx 0.1au.$, we obtain $\delta z \approx 0.5au.$. The reduction of the coherence width of the incident wavepacket is shown in Fig. 2. The width of the wavepacket is reduced dramatically due to stochastic momentum transfer with the LiF surface. In a wide energy range, the resulting wavepackets can be approximated by Eq. 11b, with $\sigma_z \approx 0.5au.$, which translates into a FWHM of $\sqrt{8\log 2}\sigma_z \approx 1.2au.$.

We determine $V_{str}(y,z)$ as the string average along the $\langle 110\rangle$ direction of the full He-LiF surface potential $V_{surf}(\vec{r})$ calculated for a large LiF cluster on the multi-configuration self consistent field level, using the quantum chemistry code Columbus [16]. The string potential along the $\langle 110\rangle$ direction is periodic with $V_{str}\left(y+d,z\right) = V_{str}(y,z)$, where d is the spacing between adjacent strings of F.

3. Calculating diffraction patterns

Due to the periodicity of the effective two-dimensional atomic string potential ($V_{str}(y,z) = V_{str}(y+d)$, where d is the space between two adjacent F or Li atoms), the interference maxima correspond to Bragg peaks,

$$k_y^{(n)} = n\frac{2\pi}{d}, \quad n = 1, 2, 3, \ldots \tag{13}$$

A typical diffraction pattern at a well-defined incident particle energy shows modulations of the intensity of the Bragg peaks.

Whether or not a particular Bragg position $k_y^{(n)}$ displays a visible interference maximum at a given energy depends on the shape of the effective atomic string potential, in particular on its corrugation amplitude.

A key parameter characterizing the diffractive scattering induced by V_{str} is the corrugation amplitude of the string potential, $(\Delta z)_{str}$ i. e. the maximum variation of the normal (z) coordinate of the equipotential surface $E_\perp = V_{str}(y,z)$. For a wide interval of normal energies (0.5 eV $\leq E_\perp \leq$ 10 eV), within which a converged potential for a large cluster can be generated, $(\Delta z)_{str}$ is remarkably weakly dependent on $E_\perp$ and essentially constant $(\Delta z)_{str} \approx 0.3$Å. As some of the experimental diffraction data are taken at even smaller perpendicular energies for ($E_\perp < 0.5$ eV), where the ab initio potential calculation becomes unreliable, we have extrapolated V_{str} to low-energy surfaces subject to the constraint that $(\Delta z)_{str}$ remains constant. Imposition of such a constraint has proven remarkably successful when compared with experimental data. As the diffraction patterns depend so sensitively on the corrugation amplitude, surface reconstruction (or buckling), i.e. the offset along the surface normal between the outermost F and the outermost Li atoms, plays an important role. The helium-LiF-potential has been calculated for a surface with a surface buckling $\delta z = 0.053$Å (i.e. the F atoms of the topmost layer being shifted towards the vacuum as compared to the Li atoms). This value was obtained in a DFT calculation and agrees with previous estimations [17, 18].

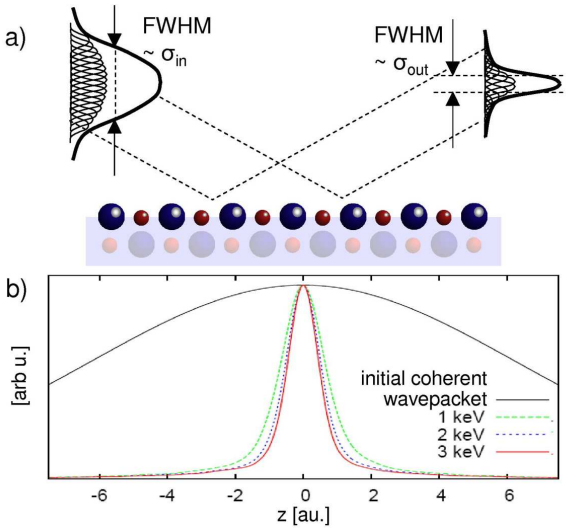

Figure 2. A delocalized wavepacket hits the surface that is considerabely wider than the size of the unit cell. Different components of the wavepacket (indicated in (a) by narrower wavepackets) are subject to different random momentum changes, which lead to a loss of coherence. The coherent width of the wavepacket is therefore drastically reduced (b).

Reconstruction of the experimental diffraction pattern requires, in addition to collisionally induced decoherence, incoherent averaging over the geometric angular divergence taken to be rectangular, W_R, and energy spread taken to be approximately, Lorentzian, W_L.

$$\langle I\left(\theta_{out},\phi_{out}\right)\rangle = \int d\theta' \int d\phi \int dE' I\left(\theta',\phi,E'\right) \times W_L\left(E'-E\right) W_R\left(\theta'-E_{out}\right) W_R\left(\theta'-\theta_{out}\right) . \quad (14)$$

We compare the resulting diffraction patterns to experimental results [4] for scattering of He atoms ($E_0 = 1$ keV) on a LiF(001) surface aligned along $\langle 110\rangle$ direction under a grazing angle of incidence $\phi_{in} = 1.1°$ ($E_\perp \approx 0.38$ eV). We find a near-perfect reconstruction of the experimental diffraction pattern without any adjustable parameter if surface buckling is taken into account (Fig. 4). The positions of the main maxima are obtained from the interference condition for a periodic potential along the y-direction,

$$\sin\alpha_n = \frac{k_y}{k_\perp} = n\frac{\lambda_{dB\perp}}{d}, \quad n = 0, \pm1, \pm2, \ldots . \quad (15)$$

The two outermost maxima are the so-called rainbow peaks. Between the rainbow peaks, there are intricate substructures, formed by additional maxima ("supernumeraries"). These structures are well reproduced by the simulation.

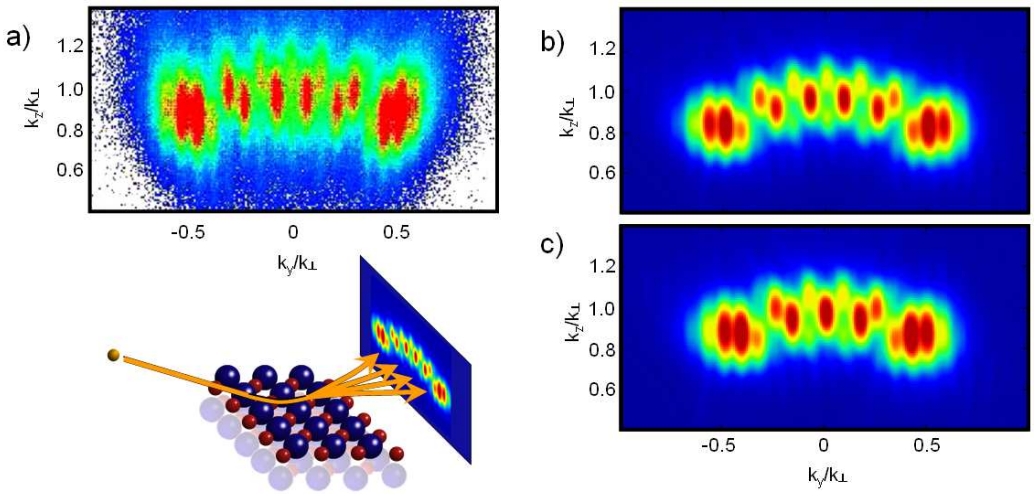

Figure 3. Experimental (from Ref. [4]) (a) and theoretical (b,c) diffraction patterns for scattering of 1keV He from LiF under $\theta = 1.1°$. In b), with surface buckling $\delta z = 0.053$Å, c) without surface buckling $\delta z = 0$. Note the different number of interference maxima.

Note that not only the number and the position of the diffraction peaks but also their width is reproduced quite accurately. The quantum trajectory Monte Carlo method allows to include momentum transfers between the projectile and the surface, so that the decohering effects are taken into account. It is important to point out that the finite peak widths are not merely a result of modifications of the atom-surface potential due to thermal vibrations. Thermal displacements of the surface atoms lead to local stochastic modifications of the atom-surface potential. They break the translation invariance of the crystal surface and lead to a reduction of the visibility of the scattering maxima. The height of the peak is reduced, which can be described by an effective Debye Waller factor, and a stochastic background of particles scattered

in random directions not corresponding to Bragg peaks emerges. This effect is visible in the elastic scattering at a disordered surface and should be distinguished from decohering effects as included in the quantum trajectory Monte Carlo method.

To illustrate this difference, we calculate the width of the zero-order peak using a hard-wall-approximation. The momentum distribution of the scattered particle, which defines the outgoing asymptotic wave measured at the detector, is proportional to a phase integral over the crystal surface [19, 20]

$$I(\mathbf{K}) \propto \int_{\mathbf{surf}} \mathbf{dR}\, \mathbf{e}^{-\mathbf{iKR}-\mathbf{i\Delta k_z}\zeta(\mathbf{R})}, \tag{16}$$

where $\mathbf{R}$ is a surface vector, $(\mathbf{K}, \mathbf{\Delta k_z})$ is the difference in momentum between the incident and the outgoing particle wave ($\mathbf{K}$ being in the surface plane and Δk_z parallel to the surface normal), and $\zeta(\mathbf{R})$ defines the equipotential plane at which the particle is scattered. The surface area over which the integration is performed, corresponds to an effective coherence length of the particle wave. For an incident plane wave, the coherence length is infinite and only momentum changes $\mathbf{K}$ corresponding to reciprocal lattice vectors are possible. In our case, the coherence length is finite and the integration extends over a finite region of the surface. $\zeta(\mathbf{R})$ is composed by adding random displacements $u(\mathbf{R})$ of the surface atoms to the equipotential plane calculated for a rigid surface without thermal vibrations. The displacements $u(\mathbf{R})$ are chosen randomly according to a distribution of thermal elongations calculated with density functional theory [21].

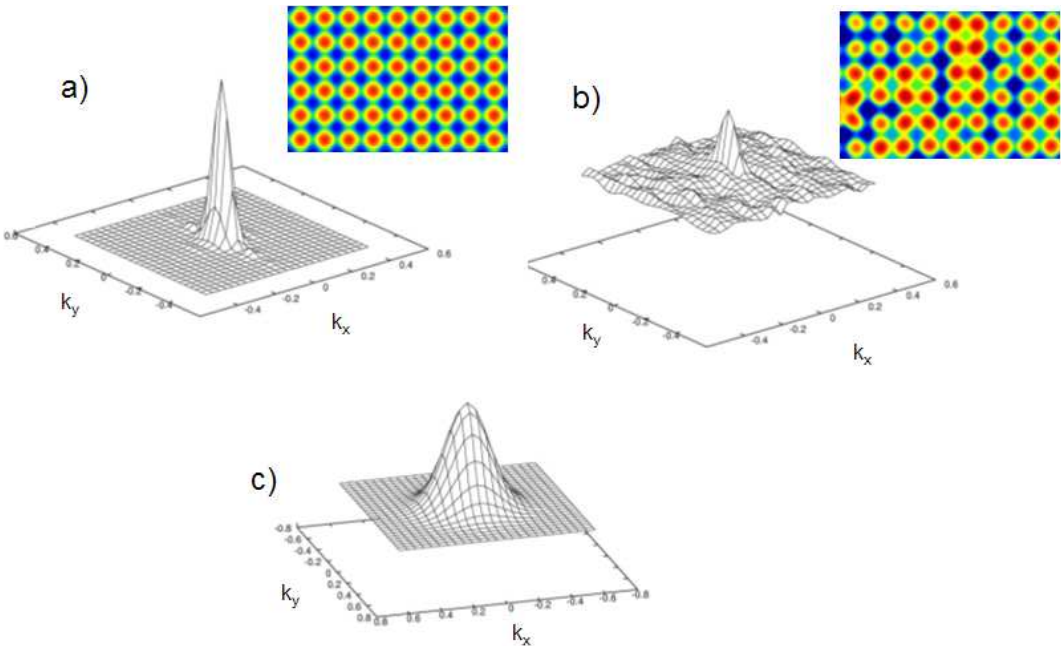

Figure 4. Momentum distributions in x and y direction (surface plane). Scattering of a wavepacket with a coherence length of 9×21 unit cells at a perpendicular energy of 400 meV exhibits a strong zeroth order diffraction peak in the absence of thermal noise(a). Averaging over 1000 random thermal displacements (b) adds noise but leaves the main peak intact. Reducing the surface area coherently illuminated by the particle (2 unit cells) changes the width of the peak drastically (c).

In Fig. 4, we show the momentum distribution $I(\mathbf{K})$ of the zeroth order peak for an ideal surface (a) and a thermally excited surface (b). The latter was calculated taking the average

of the integrations over 1000 stochastic realizations of the thermally disordered surface. In Fig. 4b, a level of "noisy" background is clearly visible, but the width of the peak itself is not changed dramatically. Its width is not primarily controlled by noise in the atom-surface potential but by the coherence width of the atomic wavepacket. Reducing the coherence width on the other hand, changes the peak drastically (Fig. 4c). In this calculation, we introduce a finite coherence length of the wavepacket by integrating over a smaller surface area (here without adding thermal fluctuations). A smaller number of unit cells contributing to the scattering process (i.e. a less sharply peaked structure factor) leads to broader diffraction peaks.

Summarizing, fast keV atomic collisions with insulating alkali-halide surfaces give rise to remarkably sharp and well-resolved diffraction images. Despite de Broglie wavelengths as small as one hundred femtometer, quantum interference persists. Due to the weak coupling of transverse and longitudinal degrees of freedom decoherence is effectively suppressed in grazing incidence collisions. Ab initio quantum trajectory Monte Carlo simulations accurately reproduce the diffraction pattern and allow to extract structural surface information such as buckling. This technique also promises application to other surfaces and structures relevant for material sciences.

Acknowledgements
We thank C. O. Reinhold, A. Schüller and H. Winter for helpful discussions. This work was supported by the FWF-Austria, grants no. SFB016 and P17359, and by the EU under contract no. HPRI-CT-2005-026015.

References

[1] Estermann I and Stern O 1930 *Z. Phys.* **61** 95
[2] Arndt M , Nairz O, Voss-Andreae J, Keller C, Van der Zouw G, and Zeilinger A 1999 *Nature* **401**, 680
Hornberger K, Uttenthaler S, Brezger B, Hackermüller L, Arndt M, and Zeilinger A 2003 *Phys. Rev. Lett.* **90**, 160401
[3] Hackermüller L, Uttenthaler S, Hornberger K, Reiger E, Brezger B, Zeilinger A, and Arndt M 2003 *Phys. Rev. Lett.* **91**, 090408
[4] Schüller A, Wethekam S, and Winter H 2007 *Phys. Rev. Lett.* **98**, 016103
[5] Schüller A, and Winter H 2008 *Phys. Rev. Lett.* **100**, 097602
[6] Rousseau P, Khemliche H, Borisov A G, and Roncin P 2007 *Phys. Rev. Lett.* **98**, 016104
[7] Aigner F, Simonovic N, Solleder B, Wirtz L, Burgdrfer J 2008 *Phys. Rev. Lett.* **101**, 253201
[8] J. Burgdörfer, in "Review of Fundamental Processes and Applications of Atoms and Ions", edited by C.D. Lin (World Scientific, Singapore, 1993)
[9] Zurek W H 1991 *Phys. Today* **44**, 36
[10] Ghirardi G C, Rimini A, and Weber T 1986 *Phys. Rev.* D **34**, 470
[11] Minami T, Reinhold C O, and Burgdörfer J 2003 *Phys. Rev.* A **67**, 022902
Seliger M*et al* 2007 *Phys. Rev.* A **75**, 032714 and Refs. therein.
[12] Desjonquères M C, Spanjaard D 1993 Concepts in Surface Physics, Springer, Berlin
[13] Dalibard J, Castin Y, and Mølmer K 1992 *Phys. Rev. Lett.* **68**, 580
Dum R, Zoller P, and Ritsch H 1992 *Phys. Rev.* A **45**, 4879
[14] Mertens A and Winter H 2000 *Phys. Rev. Lett.* **85**, 2825
Pfandzelter R, Mertens A, and Winter H 2001 *Phys. Lett.* A **290**, 145
Roberts J G, Van Hove M A, Somorjai G A 2002 *Surf. Sci.* **518**, 49
[15] Kupfer E, Gabriel H, and Burgdörfer J 1981 *Z. Phys.* A **300**, 35
Kimura K, Ida H, Fritz M and Mannami M 1996 *Phys. Rev. Lett.* **76**, 3850
[16] Lischka H et al. 2006 computer code COLUMBUS, Release 5.9
[17] De Wette F W, Kress W, and Schröder U 1985 *Phys. Rev.* B **32**, 4143
[18] Vogt J, and Weiss H, *Surf. Sci.* **501** 203
[19] Manson J R, Khemliche H, and Roncin P *Phys. Rev. Lett.* **78**, 155408
[20] Garibaldi U, Levi A C, Spadacini R and Tommei G E *Surf. Sci.* **48** 649
[21] Wirtz L, private communication